A Framework for Electrified Propulsion Architecture and Operation Analysis

Gokcin Cinar, Elena Garcia, Dimitri N. Mavris
Aerospace Systems Design Laboratory
Georgia Institute of Technology
Atlanta, GA
UNITED STATES OF AMERICA

gokcin.cinar@gatech.edu, elena.garcia@ae.gatech.edu, dimitri.mavris@aerospace.gatech.edu

Keywords: *Hybrid/Electric Propulsion Systems Architectures, electrified aircraft, subsystems, hybridization, hybrid operation*

ABSTRACT

The purpose of this research was to create a generic and flexible framework for the exploration, evaluation and side by side comparison of novel propulsion architectures. The intent for these evaluations was to account for varying operation strategies and to support architectural design space decisions, at the conceptual design stages, rather than single point design solutions. To this end, main propulsion subsystems were categorized into energy, power and thrust sources. Two types of matrices, namely the Property and Interdependency Matrices, were created to describe the relationships and power flows among these sources. These matrices were used to define various electrified propulsion architectures, including but not limited to turboelectric, series-parallel and distributed electric propulsion configurations. As a case study, the matrices were used to generate and operate the distributed electric propulsion architecture of NASA's X-57 Mod IV aircraft concept. The mission performance results were validated against the data obtained from literature. Various mission scenarios were simulated to showcase how the introduced matrices can be utilized to create and evaluate different power management schemes under changing operation strategies. It was demonstrated that this new framework facilitates rapid, automated and analysis-based comparisons among unconventional propulsion architectures where solutions are driven by requirements. The use of Property and Interdependency Matrices enables requirement and mission adaptive power management schemes, which is particularly relevant for multi-mission unmanned aerial vehicles in military applications.

1.0 INTRODUCTION

Electrified aircraft (both fully electric and hybrid electric) pose a significant architecture challenge, as both of these concepts – fully electric aircraft and hybrid electric aircraft – not only deal with considerably high electrical loads but are also extremely weight-sensitive (Isikveren et al., 2012). To overcome this challenge, various propulsion architectures have been proposed in literature, such as parallel hybrid electric, turboelectric, and distributed electric configurations.

Propulsion architectures mainly vary based on size class and desired mission capabilities. For instance, the 2-seater Pipistrel Alpha Electro[1] and Airbus E-Fan 2.0 are two successfully flown examples of purely electric aircraft concepts. Alpha Electro is powered by a single electric motor, whereas E-Fan 2.0 has twin motors, both powered by rechargeable batteries. (Borer et al., 2016) E-Fan had two hybrid electric variations over the years: E-Fan Plus included a two-stroke internal combustion engine in addition to E-Fan's twin electric motors; whereas E-Fan X is a substantially different technology demonstrator based on the BAe 146 with one of the four gas turbine engines replaced by a megawatt-class electric motor. (Siemens et al., 2017)

The 12-seater Zunum Aero[2] consists of a turboshaft engine coupled with an electric generator along with rechargeable battery packs connected in a series hybrid configuration. NASA's STARC-ABL is a single aisle commercial transport aircraft which employs a turboelectric configuration powered by twin underwing mounted turbofan engines sending power to a boundary layer ingesting fan at the tail through generators. (Welstead et al., 2016) Unlike the Zunum Aero, this concept does not employ batteries.

NASA X-57 initiated the 'Maxwell' project where the Tecnam P2006T aircraft is planned to undergo several "modifications", namely Mods I, II, III and IV, to demonstrate the benefits of distributed electric propulsion. Mod I is the Tecnam P2006T used as a baseline. In Mod II, the baseline aircraft's engines are replaced with two 60 kW motors run by a rechargeable battery. In Mod III, the baseline wing is replaced with a high-aspect ratio wing. Mod IV employs a distributed electric propulsion (DEP) architecture featuring 12 high-lift motors along the leading edge of the wing, and 2 cruise motors at the wing tips. Mod IV aims to demonstrate five-fold reduction in energy through the DEP concept compared to the baseline aircraft. (Gibbs, 2018; Schnulo et al., 2018)

The use of electricity can be particularly appealing in military unmanned aerial vehicles (UAVs). For instance, modular battery packs can be utilized to accommodate different mission strategies; or electric power can be favoured to reduce the heat signature and/or noise of the aircraft during strategic parts of a flight mission. Although there exists many small hybrid/electric UAVs, publicly available information on medium to large size concepts is scarce. One example is the medium altitude long endurance Yabhon United 40 UAV, being developed by ADCOM Systems, a company based in the UAE. It is claimed that United 40 can conduct a variety of missions with its 115 HP Rotax 914 UL engine and 80 HP electric motor.[3] The authors could not confirm the propulsion system specifications due to the lack of publicly available data at the time of this research.

Evidently, each of these examples employ a different propulsion architecture. There exist many other different electrified propulsion architectures in literature. Some examples are notionally demonstrated in Figure 1-1. Figure 1-1-(a) represents a series (also referred to as turboelectric when the fuel burning engine is a gas turbine engine) configuration where the energy that must be supplied to the propeller solely depends on the chemical energy of the fuel. By simply adding a battery to this configuration, one obtains the series hybrid configuration with an additional energy source as shown in Figure 1-1-(b), where the operation strategy suddenly becomes important since there are two different energy sources (fuel and battery) in the system. Figure 1-1-(c) connects the engine to the propeller. The power coming from the engine is split between the propeller and the motor. This means that an additional operation strategy is needed to control this split, in addition to the energy budgeting between the fuel and the battery. Figure 1-1-(d) shows a distributed series propulsion, where the power coming from the engine is distributed amongst four pathways.

[1] https://www.pipistrel-usa.com/alpha-electro/ (accessed 17 May 2019)
[2] https://zunum.aero/aircraft/ (accessed 17 May 2019)
[3] https://www.airforce-technology.com/projects/yabhon-united-40-smart-eye-2-uav/ (accessed 5 September 2019)

More variations can be easily obtained by adding new subsystems or connections to these example architectures. Although such changes might be seen as slight modifications to the propulsion system, they create new degrees of freedom in terms of operation strategies. The architecture itself gets more and more complex; thus performs differently under the same mission requirements.

Because electrified propulsion technology is still in its early stages of development, the aforementioned studies generally focus on individual examples as technology demonstrators of a particular architecture, and further analyses are conducted on a pre-selected single point design. Even in the multi-phase NASA X-57 program, the main objective is to explore the benefits of DEP specifically, and the findings will be compared against a single baseline, but not against more distinct architectures such as hybrid configurations.

The choice of a particular architecture can be based on various performance characteristics, yet a thorough comparison of different architectures and how a specific architecture is selected for the desired performance characteristics is missing. This can be due to the fact that such architectures must be created and compared very early at the aircraft conceptual design stage where design flexibility is maximum but the knowledge about the design is very limited.

Furthermore, these novel propulsion architectures enable various power management strategies which can vary throughout the mission. The optimal power management strategy may be different for two different architectures employed in otherwise the same aircraft design under the same mission requirements. This opens up a new degree of freedom: architectural comparisons are only meaningful provided that the candidate architectures are evaluated while being operated under their optimal power management schedule. Thus, operation strategy is as important as the architecture set up and they should be considered as two complementing parts when evaluating and comparing aircraft mission performance.

As a result, there is a need for a methodology to capture and compare various electrified propulsion architectures and operation strategies at early phases of design, so that important design decisions can be made based on an architectural design space, rather than single-point design solutions. Such a methodology should be generic and flexible to capture distinct and unconventional alternatives and operational strategies. This can be achieved through a model-based systems engineering approach, where architecting is done based on analysis and the solutions are driven by the requirements.

1.1 Electric Propulsion Architecture Sizing and Synthesis (E-PASS)

In the remainder of this paper, the authors describe a framework created to rapidly generate, modify and evaluate architecture definitions and operational strategies. This framework is one of the building blocks of an in-house sizing and synthesis tool, called “Electric Propulsion Architecture Sizing and Synthesis”, or E-PASS, which enables design and performance evaluation of any vehicle design, including but not limited to electric and hybrid electric aircraft, and allows for rapid comparisons between diverse propulsion architectures. (Cinar, 2018) However, the framework described here is tool-agnostic and can be applied within other mission analysis approaches.

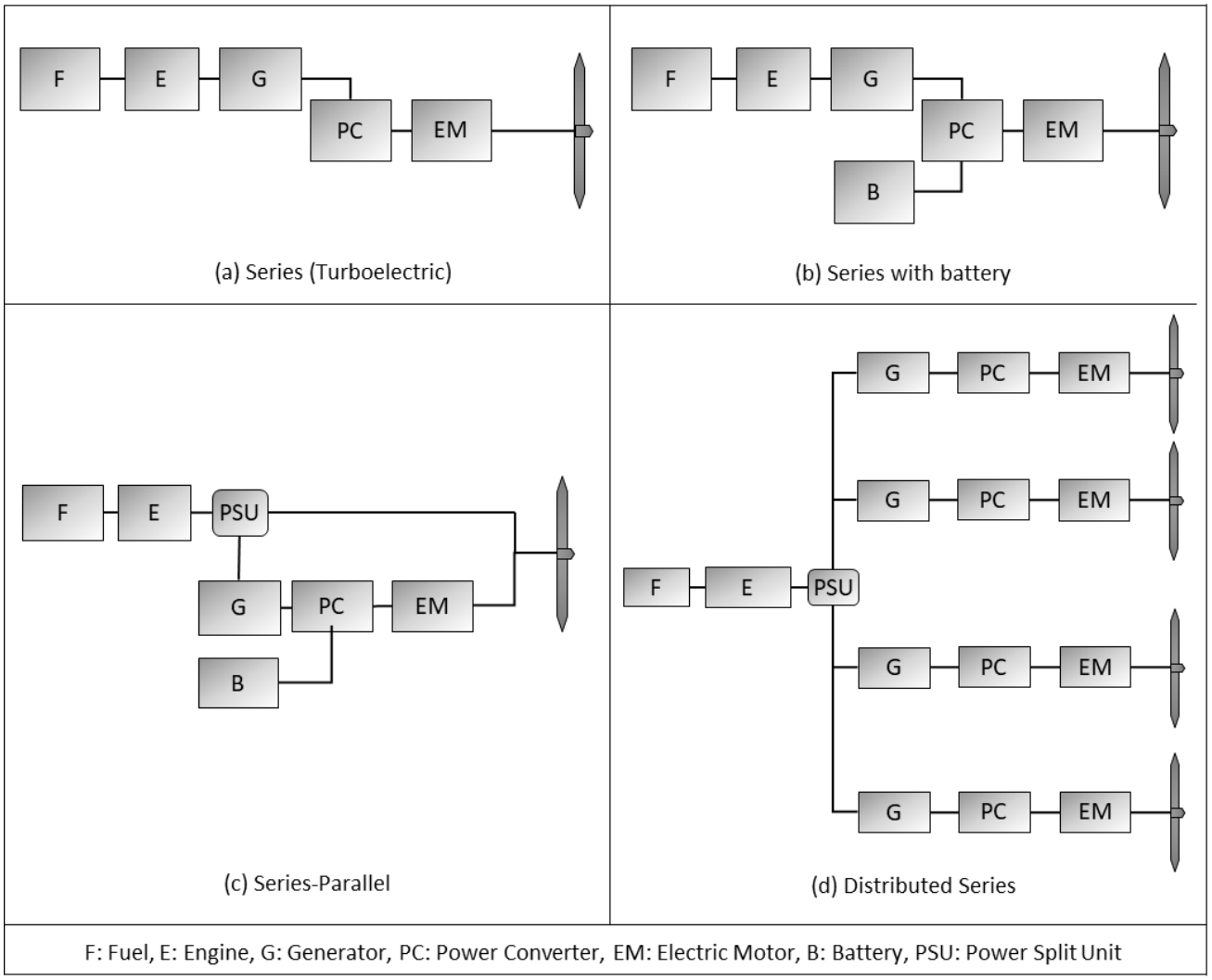

Figure 1-1 Notional series configurations used in different hybrid electric propulsion architectures.

E-PASS can be used to size a notional aircraft configuration with a new propulsion architecture (on-design mode) or evaluate the mission performance of an existing concept without sizing it (off-design mode). It has built-in physics-based subsystem models, component-based weight estimation techniques, power management optimizer and a generic mission analysis module which allows mission performance evaluations of any propulsion architecture.

The building blocks of E-PASS are shown in Figure 2.1-1. This paper focuses mainly on Blocks 2 and 5, namely the subsystem architecture definition and power management strategy. The interested reader can refer to Cinar (2018) for a more detailed description of the working principles of the remaining blocks.

2.0 DEVELOPMENT OF A MATRIX-BASED PROPULSION ARCHITECTURE AND OPERATION FRAMEWORK

As discussed in the previous chapter, there are two parts to the architecture comparison problem: (i) architecture setup, where its components (i.e. power generation and distribution subsystems, or PGDS) are defined and physical connections between them are established; and (ii) operation (i.e. power management) strategy, where the power flow through these subsystems are defined as a function of time.
This paper introduces a new way of establishing the setup and operation of an architecture through Property and Interdependency Matrices.

2.1 Property and Interdependency Matrices

In any given architecture, subsystems interact with each other and impact each other's properties. In this context, a property of a subsystem is defined as a quality, trait or attribute which can be calculated through physics-based models and conservation laws in mission performance analysis based on the state of the vehicle and the interactions between subsystems. Interdependencies are a result of the necessary connections to create a power flow path to propagate the properties.

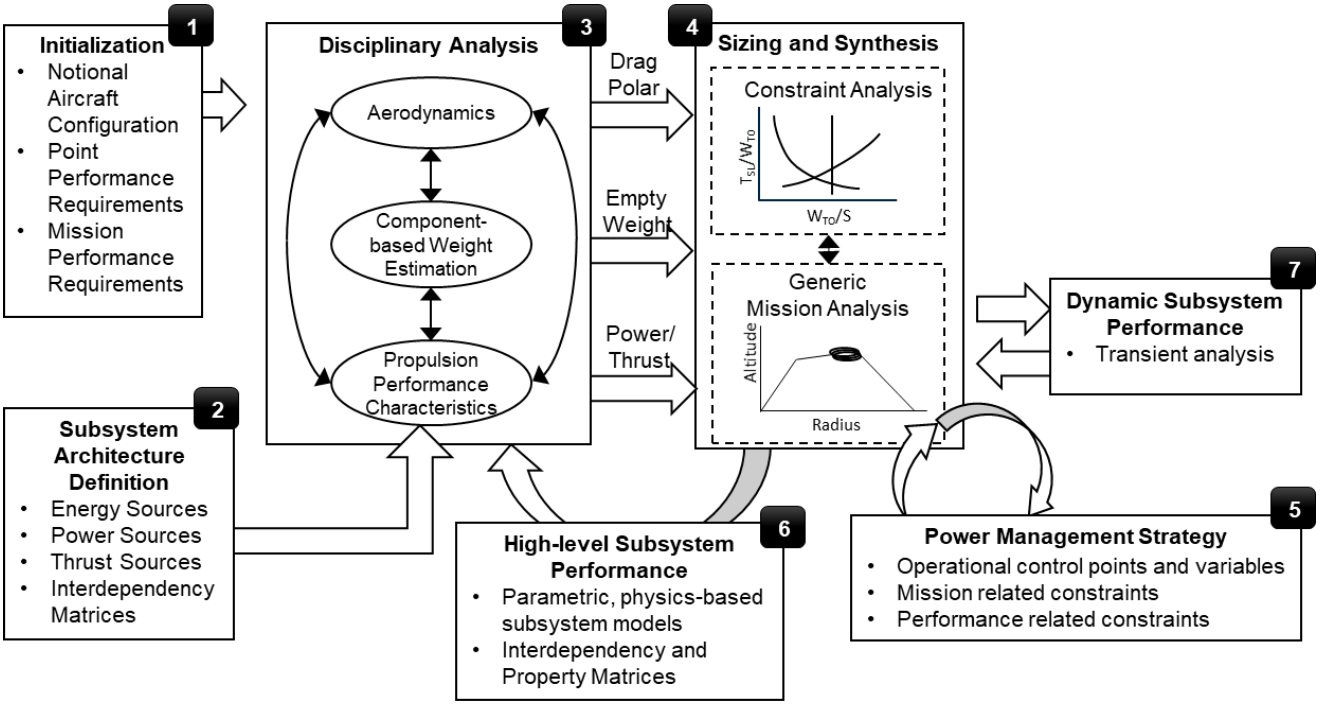

Figure 2.1-1 Building blocks of the methodological framework: E-PASS.

Property and Interdependency Matrices (matrices ***A*** and ***B***, respectively) represent two types of matrices enabling a systematic way of allocating the top-level requirements to subsystem level resources. Although these matrices can be defined for all PGDS, we will prove how choosing a specific group of PGDS enable rapid architecture definitions at early phases of conceptual design, by avoiding redundancy and without losing generalizability.

It has been discussed in recent publications (and also inherently shown in Figure 1-1.) that different propulsion architectures can be created using similar PGDS, which can be integrated through various configurations to create diverse architectures. (Cinar et al., 2017 and Cinar 2018). Further inspections showed that all architectures consist of three main sources which are necessary and sufficient to describe an architecture.

The three main sources that must be employed in a propulsion system architecture are:

1. **Power source (PS):** any subsystem that generates primary (propulsive) power (e.g. electric motor, internal combustion engine, turboshaft engine, etc.)

2. **Thrust source (TS):** any subsystem that generates thrust (e.g. propeller, fan, etc.)

3. **Energy source (ES):** any subsystem that stores energy to be used by the primary power sources (e.g. batteries, fossil fuel, fuel cells, etc.)

PGDS which are mapped to the three source categories are enumerated by identification numbers (IDs) to ensure traceability and provide convenience, as shown in Figure 2.1-2. Once the properties of these sources and their relationships with each other are defined, remaining PGDS (such as power converters, generators, cables, etc.) can be heuristically placed in between these sources. Such heuristics are planned to be added to E-PASS as a future work, and are not in the scope of this paper.

Based on the diverse architectures discussed in the Introduction section, three main types of connections, or 'interdependencies' were established between (i) power sources and energy sources (PSES), (ii) driven power sources and driving power sources (PSPS), and (iii) power sources and thrust sources (PSTS), as depicted in Figure 2.1-2.

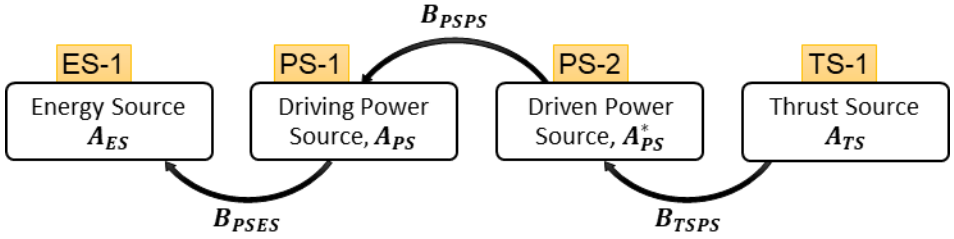

Figure 2.1-2 Property propagation from upstream to downstream sources by Interdependency and Property Matrices.

The interdependency matrices were originally introduced by the lead author in in Cinar (2018). This paper builds on those definitions to create a more convenient and generalizable set of Interdependency Matrices. These are defined as:

1. **Power Source – Energy Source Matrix (B_{PSES}):** lays out which power source gets its energy from which energy source.

2. **(Driven) Power Source – (Driving) Power Source Matrix (B_{PSPS}):** distinguishes the connected power sources by laying out the 'driving' power sources (i.e. power sources which transfer a portion or all of its energy to another power source, shown in columns) against 'driven' power sources (i.e. power sources

which gets a portion or all of its energy from another power source, shown in rows). By definition, each power source drives itself, and thus the diagonal of this matrix is always 1.

3. **Thrust Source – Power Source Matrix ($\boldsymbol{B_{TSPS}}$)**: lays out which thrust source is directly connected to which power source.

Table 2.2-1 expands the Interdependency and Property Matrices for a propulsion architecture which consists of *j* number of energy sources, k number of power sources, and l number of thrust sources. There are n number of mission points between which the state of flight is assumed to be frozen.

In a Property Matrix, same type sources are distinguished by matrix columns based on their IDs. The variation in a source property at different mission points is shown in matrix rows. In Interdependency Matrices, the naming convention is "rows-to-columns"; for instance, in $\boldsymbol{B_{TSPS}}$, TS are distributed to the rows, and PS to the columns.

These two types of matrices can be written for any variable *a* or *b* to construct and operate any propulsion architecture. They can be utilized within the mission analysis functions of E-PASS, as will be later shown in Eqns (4)-(7).

2.2 Architecture Construction

The Interdependency Matrices can be directly used to create various architectures, and explore configurations that were not thought of before. This can be achieved by assigning logical ones (true) and zeros (false) to the elements of an Interdependency Matrix to describe whether a source is logically connected to another or not. This special form of the Interdependency Matrices will be called Architecture Matrices, $\boldsymbol{B^A_{TSPS}}$, $\boldsymbol{B^A_{PSPS}}$, and $\boldsymbol{B^A_{PSES}}$.

Table 2.2-1 Interdependency and Property Matrix Formats.

	Thrust Source – Power Source	**(Driven) Power Source – (Driving) Power Source**	**Power Source – Energy Source**
Interdependency Matrices, B^b	$B^b_{TSPS} = \begin{bmatrix} b_{TS-1,PS-1} & \cdots & b_{TS-1,PS-k} \\ \vdots & \ddots & \vdots \\ b_{TS-l,PS-1} & \cdots & b_{TS-l,PS-k} \end{bmatrix}$	$B^b_{PSPS} = \begin{bmatrix} b_{PS-1,PS-1} & \cdots & b_{PS-1,PS-k} \\ \vdots & \ddots & \vdots \\ b_{PS-k,PS-1} & \cdots & b_{PS-k,PS-k} \end{bmatrix}$	$B^b_{PSES} = \begin{bmatrix} b_{PS-1,ES-1} & \cdots & b_{PS-1,ES-j} \\ \vdots & \ddots & \vdots \\ b_{PS-k,ES-1} & \cdots & b_{PS-k,ES-j} \end{bmatrix}$
	Thrust Sources	**Power Sources**	**Energy Sources**
Property Matrices, A^a	$A^a_{TS} = \begin{bmatrix} a_{TS-1,n=1} & \cdots & a_{TS-l,n=1} \\ \vdots & \ddots & \vdots \\ a_{TS-1,n} & \cdots & a_{TS-l,n} \end{bmatrix}$	$A^a_{PS} = \begin{bmatrix} a_{PS-1,n=1} & \cdots & a_{PS-k,n=1} \\ \vdots & \ddots & \vdots \\ a_{PS-1,n} & \cdots & a_{PS-k,n} \end{bmatrix}$	$A^a_{ES} = \begin{bmatrix} a_{ES-1,n=1} & \cdots & a_{ES-j,n=1} \\ \vdots & \ddots & \vdots \\ a_{ES-1,n} & \cdots & a_{ES-j,n} \end{bmatrix}$

To serve as an example of how these matrices can be used to set up new architectures, each configuration in Figure 2.3-1 is accompanied by its Architecture Matrices. According to the above definitions, the

Interdependency matrices given for the configuration in Figure 2.3-1-(a) read as "*"$\boldsymbol{B_{PSES}}$: ES-1 supplies energy to PS-1"*; *"$\boldsymbol{B_{PSPS}}$: PS-1 drives PS-2"*; *"$\boldsymbol{B_{TSPS}}$: TS-1 is powered by PS-2"*.

As it can be seen from Figure 2.3-1, each architecture can be uniquely expressed with a specific set of Architecture Matrices. As a future work, the authors will explore unconventional architectures by setting up combinatorial problems using these matrices.

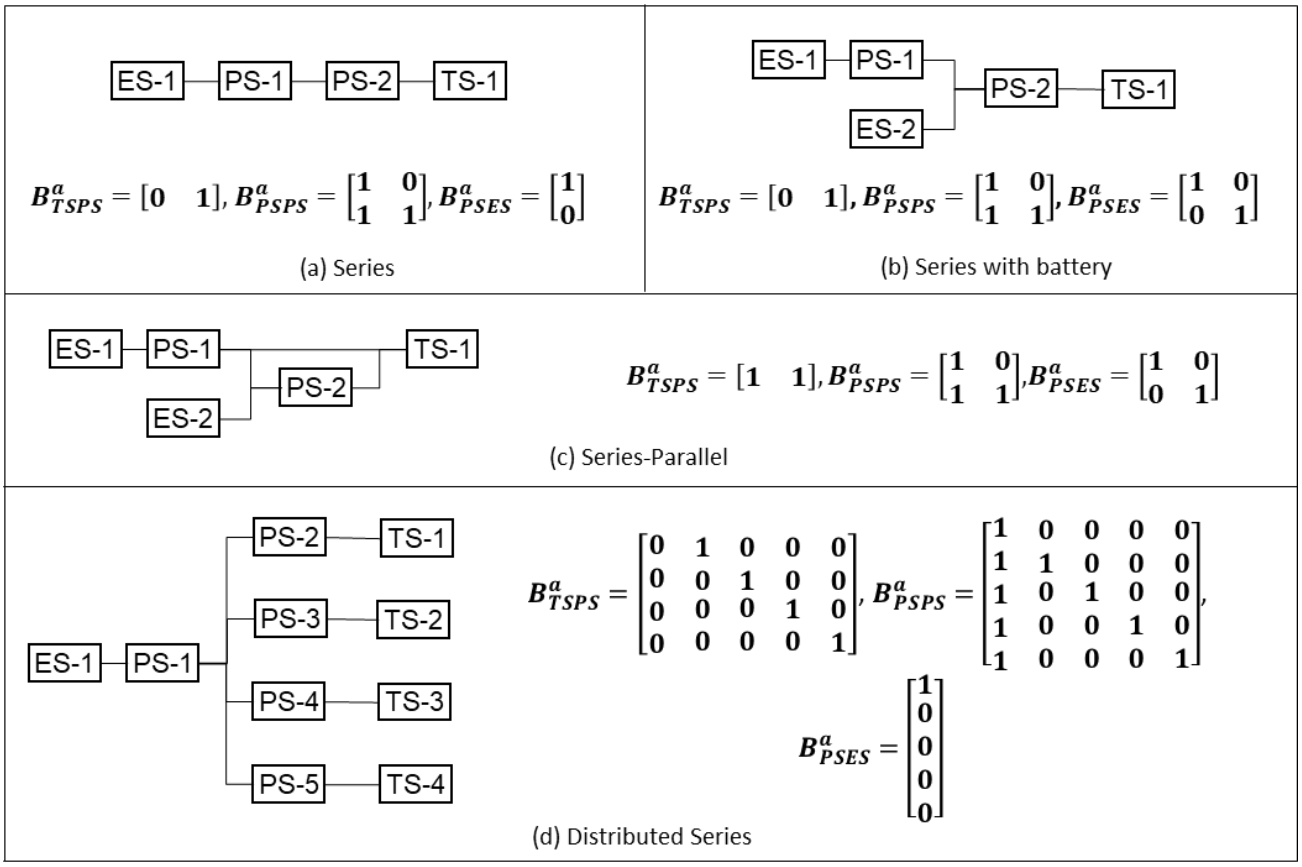

Figure 2.3-1 Configurations in Figure 1-1 recreated with three source categories and Interdependency matrices.

2.3 Architecture Operation

The Interdependency and Property Matrices can also be used to apply and change strategies during the flight mission. Generally speaking, if a propulsion architecture consists of multiple subsystems of the same source category, then the propulsion system can be utilized differently for varying requirements, since such connections create potential splits in power flows. For instance, in Figure 2.3-1-(c), there are two power and two energy sources. Although PS are connected in series, they can also contribute to the thrust power independently. Moreover, energy required to drive PS-2 can be supplied by either the battery or the engine (through a generator), or both as a combination.

The utilization of power flow paths can vary throughout the mission. In this work, the operation strategy of each source throughout the mission is described by *operational control points* and *variables*.

2.3.1 Operational Control Points

Operational control points are instances within the mission profile where the operation strategy is varied. Figure 2.3.1-1 shows a notional mission profile where mission legs are separated by mission points. In this example, three operational control points were placed at the beginning of climb, beginning of cruise, and end of cruise.

A set of control variables is assigned to each control point to define the power management strategy starting from that point up until the next point. These points can be placed in the mission profile based on desired thresholds put on flight conditions, such as altitude, weight, energy spent, etc. One can generate as many control points as one likes to change the operation strategy more frequently. However, if the power management is to be optimized, then denser control points lead to longer optimization times. Moreover, there is no particular reason to believe that the power management strategy would change frequently within each mission segment, and thus the control points should be placed where a change is expected to occur.

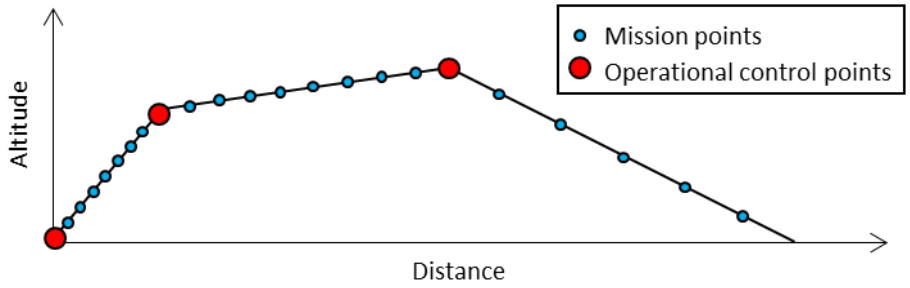

Figure 2.3.1-1 An example placement of operational control points on a notional mission profile.

2.3.2 Operational Control Points

An operational control variable, λ_{XY}, is defined as the ratio of the power contribution of Source X to the power required to run an upstream Source Y that is directly connected to X, as shown in Eqn (1):

$$\boldsymbol{\lambda_{XY} = P_{contribution\ of\ X\ to\ Y} / P_{Y,req}} \quad \textbf{(1)}$$

where $\boldsymbol{P}$ is power.

Control variables for all possible source-to-source connections can be written in terms of Interdependency Matrices. The new matrices created from Interdependency Matrices given in Table 2.2-1 are called the Operation Matrices $\boldsymbol{B^{\lambda}_{TSPS}}$, $\boldsymbol{B^{\lambda}_{PSPS}}$, and $\boldsymbol{B^{\lambda}_{PSES}}$, which consist of control variables between the specified sources.

For instance, for the architecture shown in Figure 2.3-1-(c), if PS-1 supplies 60% of the power required to run TS-1, then $\boldsymbol{B^{\lambda}_{TSPS}}$ becomes:

$$\boldsymbol{B^{\lambda}_{TSPS} = [\lambda_{TS1,PS1} \quad \lambda_{TS1,PS1}] = [0.6 \quad 0.4]} \quad \textbf{(2)}$$

Notice that each row of Operation Matrices must add up to 1 to supply 100% of the power required by the upstream source.

The connections in Operation Matrices must obey the physical connection rules given by the Architectural Matrices. A disconnected source-to-source couple cannot be assigned a control variable. However, on contrary to the Architecture Matrices, elements of Operation Matrices can take different values during the mission at the aforementioned control points.

In addition to the source-to-source matrices given in Table 2.2-1, a matrix $\boldsymbol{B}^{\boldsymbol{\lambda}}_{\boldsymbol{TS}\infty}$ must be defined for the required thrust power split between all TS. $\boldsymbol{B}^{\boldsymbol{\lambda}}_{\boldsymbol{TS}\infty}$ is a 1-by-*l* matrix where columns represent different TS. In this case, the upstream power requirement is the thrust power required based on the desired mission performance.

2.4 Matrix-based Generic Mission Analysis

This section shows how the established matrices can be used within mission performance analysis. A set of equations are laid out to calculate the power flow in any architecture configuration.

The most upstream power required is the overall required thrust power, $(TV)_{req}$, is given by Eqn (3):

$$(\boldsymbol{TV})_{\boldsymbol{req}} = \boldsymbol{DV} + \frac{\boldsymbol{d}}{\boldsymbol{dt}}\left(\boldsymbol{Wh} + \frac{\boldsymbol{1}}{\boldsymbol{2}}\frac{\boldsymbol{W}}{\boldsymbol{g}}\boldsymbol{V^2}\right) \quad \textbf{(3)}$$

where *D* is drag, *V* is airspeed, *t* is time, *W* is weight, *h* is altitude and *g* is the gravitational acceleration. These variables are written as a 1-by-*n* matrix (similar to Property Matrices but with a single column) for n number of mission points, with the operations in Eqn (3) converted to element-wise operations.

Next, going from the most upstream to the downstream, i.e. following the property propagation direction shown in Figure 2.1-2, power required from each source is computed using Equations (4)-(7). It is assumed that the control variables are pre-given as a result of a power split strategy or an optimization problem.

$$\boldsymbol{A}^{\boldsymbol{P}}_{\boldsymbol{TS}} = (\boldsymbol{TV})_{\boldsymbol{req}}\boldsymbol{B}^{\boldsymbol{\lambda}}_{\boldsymbol{TS}\infty} \quad \textbf{(4)}$$

$$\boldsymbol{A}^{\boldsymbol{P^*}}_{\boldsymbol{PS}} = \boldsymbol{A}^{\boldsymbol{P}}_{\boldsymbol{TS}}(\boldsymbol{B}^{\boldsymbol{\lambda}}_{\boldsymbol{TSPS}} \oslash \boldsymbol{B}^{\boldsymbol{\Pi}}_{\boldsymbol{TSPS}}) \quad \textbf{(5)}$$

$$\boldsymbol{A}^{\boldsymbol{P}}_{\boldsymbol{PS}} = \boldsymbol{A}^{\boldsymbol{P^*}}_{\boldsymbol{PS}}(\boldsymbol{B}^{\boldsymbol{\lambda}}_{\boldsymbol{PSPS}} \oslash \boldsymbol{B}^{\boldsymbol{\Pi}}_{\boldsymbol{PSPS}}) \quad \textbf{(6)}$$

$$\boldsymbol{A}^{\boldsymbol{P}}_{\boldsymbol{ES}} = \boldsymbol{A}^{\boldsymbol{P}}_{\boldsymbol{PS}}(\boldsymbol{B}^{\boldsymbol{\lambda}}_{\boldsymbol{PSES}} \oslash \boldsymbol{B}^{\boldsymbol{\Pi}}_{\boldsymbol{PSES}}) \quad \textbf{(7)}$$

where $\boldsymbol{A}^{\boldsymbol{P}}_{\boldsymbol{TS}}, \boldsymbol{A}^{\boldsymbol{P^*}}_{\boldsymbol{PS}}, \boldsymbol{A}^{\boldsymbol{P}}_{\boldsymbol{PS}}$, and $\boldsymbol{A}^{\boldsymbol{P}}_{\boldsymbol{ES}}$ are property matrices of power required, $\boldsymbol{B}^{\boldsymbol{\Pi}}_{\boldsymbol{TSPS}}, \boldsymbol{B}^{\boldsymbol{\Pi}}_{\boldsymbol{PSPS}}$, and $\boldsymbol{B}^{\boldsymbol{\Pi}}_{\boldsymbol{PSES}}$ are interdependency matrices of power path efficiencies between the sources designated in the subscripts, and $\oslash$ is the elementwise division operator.

A power path efficiency, Π, is the multiplication of efficiency factors of all PGDS on a specific power path (e.g. cables, power split units, gearboxes, etc.). (Nam et al., 2005). As Π can change throughout the mission, path efficiencies used in Equations (5)-(7) are defined as interdependency matrices where each element represents the path efficiency between the two sources specified by the row and column numbers. The path efficiency also includes the efficiency of the immediate upstream source. Efficiency of a non-existing source-to-source connection is assigned a dummy value of 1 to avoid division by zero. This assignment is dummy as the non-existing connection vanishes during calculations thanks to the Operation Matrix. Interdependency matrices created for path efficiencies can change value at each mission point.

It must be noted that in Eqn (5) is an intermediate step to calculate the required power from the sources connected to TS only, designated by $\boldsymbol{A_{PS}^{P^*}}$. The actual total power required from each PS is then calculated in Eqn (6) as $\boldsymbol{A_{PS}^{P}}$, which includes both the driving and driven PS power requirements thanks to the matrix multiplications which lay out the pre-specified connections through the interdependency matrices, without requiring any manual interference.

Equations (4)-(7) are just an example of how Property Matrices can be utilized with Interdependency Matrices within mission analysis to calculate power required from each source. An example on how these matrices are expanded based on the architecture is given in the appendix. The approach shown here is generalizable, and can be used to calculate other properties, such as energy to recharge batteries in suitable architectures.

To conclude, Property and Interdependency Matrices can be used to convert any property of a source type to the same property of another source type through matrix multiplications. Without these matrices, such equations would have to be manually adjusted based on the architecture. Therefore, these matrices bring computational power and ease of use, both of which are needed to evaluate architectures and their operations in batches in early design stages. With the use of the matrices, this framework enables adaptive power management, which could be of particular interest for multi-mission military UAVs.

3.0 EXAMPLE RESULTS FOR NASA X-57 MOD-IV AIRCRAFT

The architecture definition and operation methods explained in this paper were integrated into Blocks 2 and 5 (shown in Figure 2.1-1) of E-PASS, respectively. E-PASS was then used to model and analyse the mission performance of the distributed electric propulsion modification of the X-57. The X-57 was selected to demonstrate the capabilities of the developed framework because there exists significant amount of data about it in public domain and it employs multiple propulsors providing different power management strategies.

All geometry, weights, propulsion, drag polar and performance data were gathered from publicly available publications. The interested reader can refer to Cinar (2018) for more details on the detailed explanations and equations used to create the source models and generic mission analysis.

X-57 employs 2 cruise motors (CM) and 12 high lift electric propulsors (HLP) with a maximum continuous power of 60 kW and 10 kW, respectively. (Schnulo et al., 2018) and Chin et al., 2017) For both motor types, a 95% peak efficiency was assumed at these power settings and loss-based electric motor models were created based on Larminie and Lowry (2012).

Two generic propeller models were created to represent the cruise and high lift propellers using blade-element momentum theory. Two battery packs were modelled as two identical energy sources with a constant discharge efficiency of 95%. (Chin et al., 2017)

The thrust, power and energy sources were connected by the Architecture Matrices given below. $\boldsymbol{B_{TSPS}^{a}}$ and $\boldsymbol{B_{PSPS}^{a}}$ are both 14-by-14 identity matrices, whereas $\boldsymbol{B_{PSES}^{a}}$ is a 14-by-2 matrix of ones, as shown in Figure 3-1.

The mission profile and power schedules of both CM and HLP are shown in Figure 3-1 based on the data obtained from Chin et al. (2017). The mission profile consists of main and reserve (diversion) missions. In this study, taxi, take-off, and landing were kept out of scope, focusing solely on the climb, cruise and descent segments as highlighted in Figure 3-2.

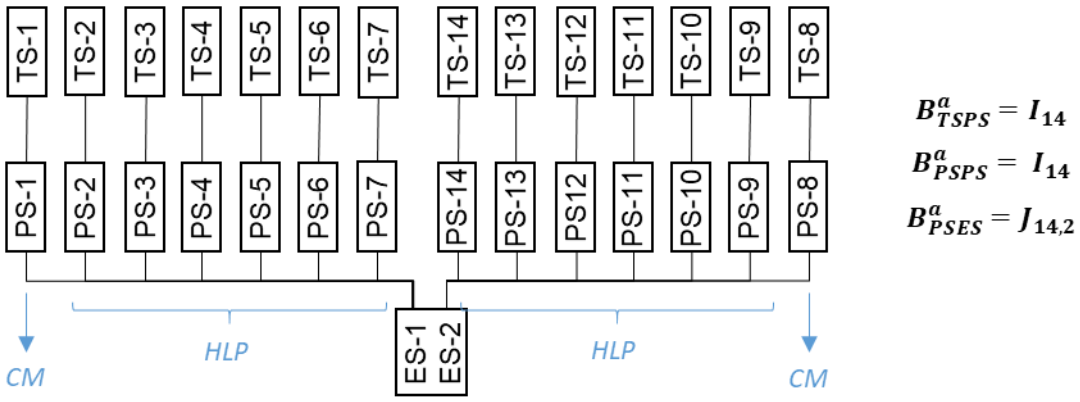

Figure 3-1 Simplified X-57 architecture based on Clarke et al. (2017) and corresponding Architecture Matrices.

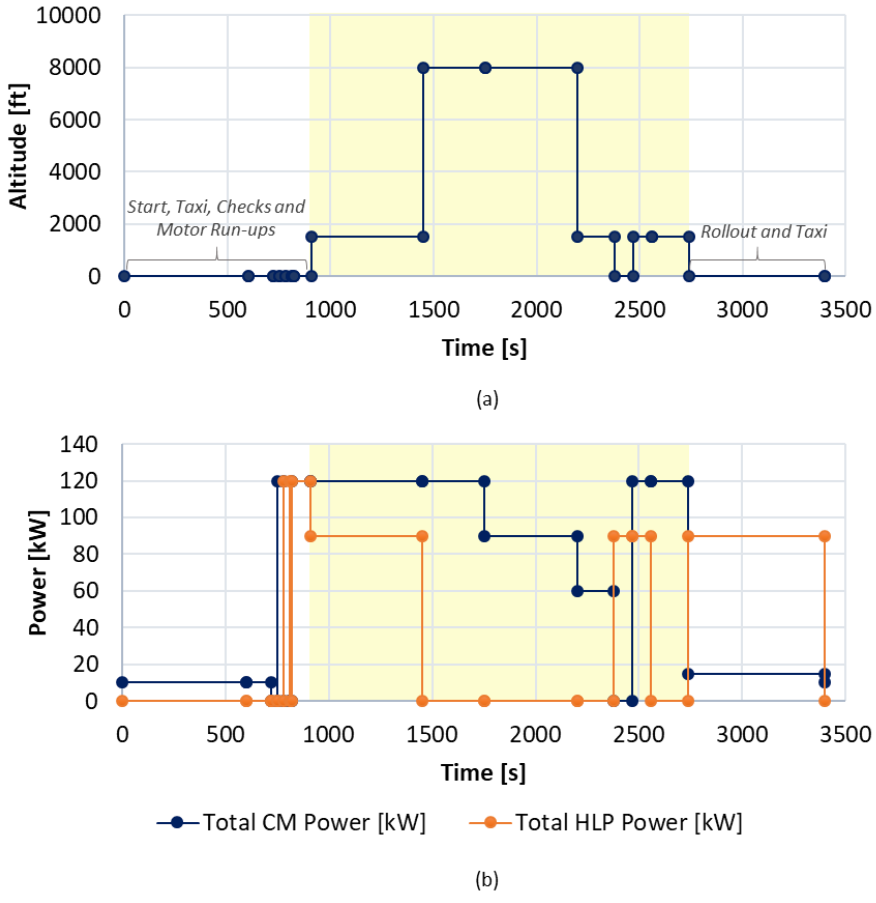

Figure 3-2 (a) Mission profile, (b) Power schedules of X-57. Data obtained from Chin et al. (2017).

The mission profile highlighted in Figure 3-2-(a) was recreated in the Generic Mission Analysis module in E-PASS based on the characteristics listed in Table 3-1. The mission analysis was set to converge on total mission time.

Table 3-1 Specified mission segment characterizations in E-PASS.

Mission Segments	Specified Characteristics
Climb	Initial and final altitude and speed, rate of climb, motor rating
Cruise	Initial altitude and speed, final altitude and speed
Descent	Initial and final altitude and speed, rate of descent, motor rating

Each point shown in Figure 3-2 corresponds to a different total power combination. The points shown in Figure 3-2-(b) were set as the 8 control points where the operation strategy is changed as a function of altitude and mission segment. 3 sets of Operation Matrices were created for each control point using the control variables shown in Table 3-2.

Table 3-2 Control points and control variables created for X-57 shown as elements of the Operation Matrices.

Mission	Control Points	Mission Segments	Altitude [ft]	$\lambda_{TS-1,\infty}$ $\lambda_{TS-8,\infty}$	$\lambda_{TS-3,\infty}$ ⋮ $\lambda_{TS-7,\infty}$ $\lambda_{TS-9,\infty}$ ⋮ $\lambda_{TS-14,\infty}$	$\lambda_{TS-1,PS-1}$ $\lambda_{TS-8,PS-8}$	$\lambda_{TS-3,PS-3}$ ⋮ $\lambda_{TS-7,PS-7}$ $\lambda_{TS-9,PS-9}$ ⋮ $\lambda_{TS-14,PS-14}$	$\lambda_{PS-1,ES-1}$ $\lambda_{PS-2,ES-1}$ ⋮ $\lambda_{PS-14,ES-1}$	$\lambda_{PS-1,ES-2}$ $\lambda_{PS-2,ES-2}$ ⋮ $\lambda_{PS-14,ES-2}$
Main	1	Climb	0	0.2857	0.0571	1	1	0.5	0.5
	2	Climb	1500	0.5	0	1	1	0.5	0.5
	3	Cruise	8000	0.5	0	1	1	0.5	0.5
	4	Descent	8000	0.5	0	1	1	0.5	0.5
	5	Descent	1500	0	0.0833	1	1	0.5	0.5
Reserve	6	Climb	0	0.2857	0.0571	1	1	0.5	0.5
	7	Cruise	1500	0.5	0	1	1	0.5	0.5
	8	Descent	1500	1	0.0833	1	1	0.5	0.5

Elements of $\boldsymbol{B}^{\boldsymbol{\lambda}}_{\boldsymbol{TS}\infty}$ were chosen based on the power distribution shown in Figure 3-2-(b). $\boldsymbol{B}^{\boldsymbol{\lambda}}_{PSTS}$ matrix stays constant throughout the operation since each TS is connected to a single PS only. Because PS are not connected to each other, $\boldsymbol{B}^{\boldsymbol{\lambda}}_{PSPS}$ is a 14-by-14 identity matrix which was not explicitly shown in the table. It was assumed that each PS draws equal amount of energy from both ES at any given time. Thus, $\boldsymbol{B}^{\boldsymbol{\lambda}}_{PSES}$ remains constant as well.

The converged mission profile and the resulting power and energy trends of various sources are shown in Figure 3-3. It can be seen by comparing Figure 3-3 to Figure 3-2 that the calculated mission performance of the X-57 model created in E-PASS is very similar to the data obtained from literature.

It must be noted that an exact performance match was not expected due to the lack of available data especially on the aerodynamic performance of the blown wing configurations. In fact, the drag polar information was obtained from Deere et al. (2017) and modified to match the power schedules given by Chin et al. (2017). Moreover, no

information could be found about the power off-takes of X-57. Thus, the power and energy plots given in Figure 3-3 only reflect those related to required thrust power.

The objective of creating the X-57 model was to demonstrate a use case scenario for the property and interdependency matrices. The power and energy plots given in Figure 3-3 were created from the power and energy property matrices calculated by Equations (3)-(7) for the given Architecture and Operation Matrices.

Different operational scenarios can be visualized by simply changing the values of the Operation Matrices given in Table 3-2. To demonstrate this capability, two motor failure scenarios during the reserve mission were analysed.

The first scenario represents an inoperative cruise motor. In this situation, Clarke et al. (2017) reports for the case for Mod III (which does not employ any HLP) that the rudder cannot counteract the resulting moment and it is better to disable both propulsors. Since the HLP in Mod IV cannot balance the moment of a single cruise motor either, both CM (PS 1 and 8) were disabled.

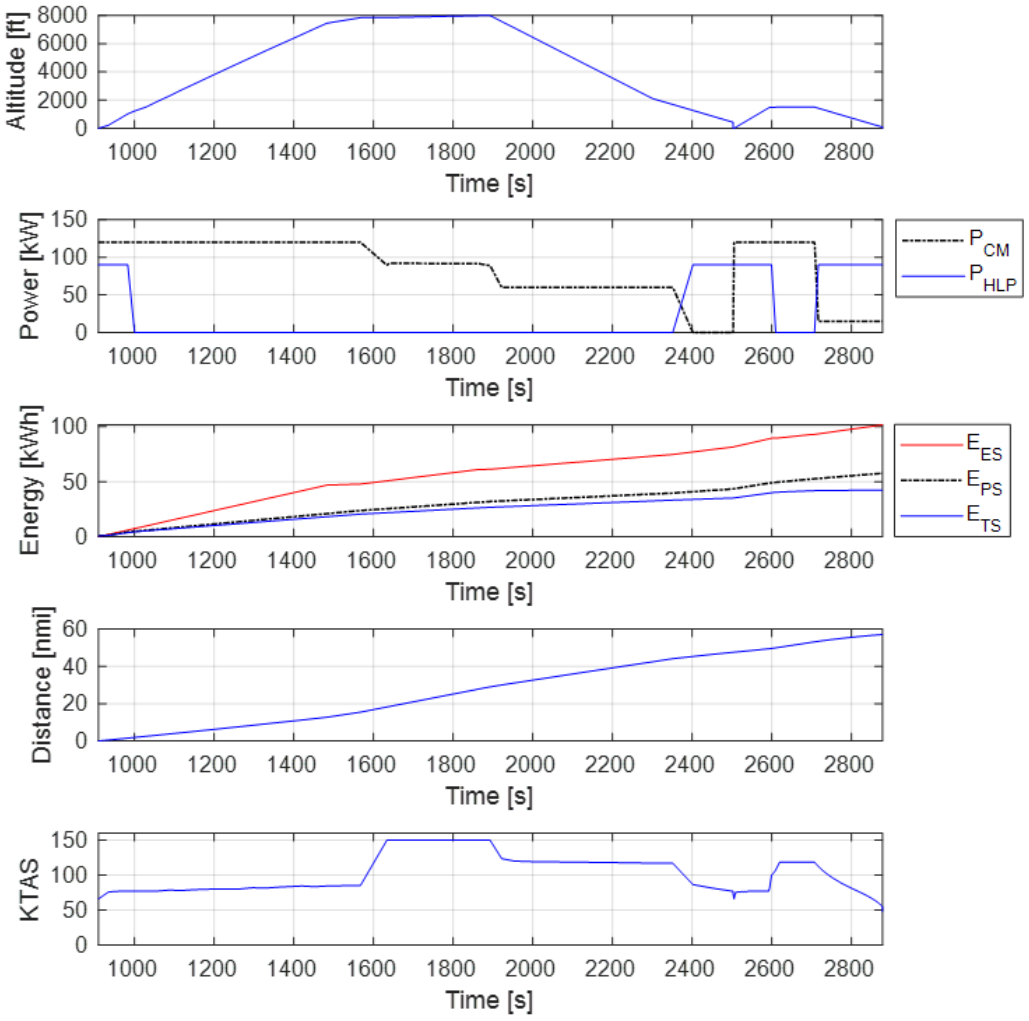

Figure 3-3 Mission performance analysis results compared to data obtained from Chin et al. (2017).

In the second scenario, the right-most HLP (PS-9 in Figure 3-1) was assumed inoperative. In this case, the total required power could be achieved by disabling the left-most HLP (PS-2) to balance out the moment due to the inoperative motor and increasing the power demand from the remaining HLP from 7.5 kW to 9 kW during the climb and descent segments.

The required thrust under these mission scenarios was distributed to the available thrust sources based on the original power schedules using the control variables given in Table 3-3. The rest of the control variables between other sources remains the same. Note that because the inoperative motors were represented by zero thrust requirement through the associated $\lambda_{TS,\infty}$, there is no need to modify the $\lambda_{TS,PS}$ given in Table 3-2. The results are given in Figure 3-4.

Table 3-3 Control variables under inoperative motor scenarios during the reserve mission.

Scenario	Control Points	Reserve Mission Segments	Altitude [ft]	$\lambda_{TS-1,\infty}$ $\lambda_{TS-8,\infty}$	$\lambda_{TS-2,\infty}$ $\lambda_{TS-9,\infty}$	$\lambda_{TS-3,\infty}$ ⋮ $\lambda_{TS-7,\infty}$	$\lambda_{TS-10,\infty}$ ⋮ $\lambda_{TS-14,\infty}$
1	6	Climb	0	0	0.0833	0.0833	0.0833
	7	Cruise	1500	0	0.0833	0.0833	0.0833
	8	Descent	1500	0	0.0833	0.0833	0.0833
2	6	Climb	0	0.2857	0	0.0429	0.0429
	7	Cruise	1500	0.5	0	0	0
	8	Descent	1500	0.2857	0	0.0429	0.0429

It must be noted that the mission performance for the hypothetical scenarios given in Figure 3-4 might not exactly match the actual performance of X-57 mostly because of the lack of aerodynamics data of the blown wing. Unfortunately, at the time of this work there was no published data for the actual performance of X-57 under these conditions to compare the results to. However, this study represents a use case to demonstrate how the changes in operation matrices resulted in a change in reserve mission characteristics and source properties.

4.0 CONCLUSION AND RECOMMENDATIONS

This paper introduced a framework created to rapidly define, evaluate and compare novel propulsion architectures though matrix-based analysis. PGDS were categorized into energy, power and thrust sources which were deemed necessary and sufficient to define any propulsion architecture. The connections between these three sources were established through Interdependency Matrices. Once the architectures were constructed, their operations were described by Property and Interdependency Matrices which can be used directly within mission performance analysis equations. The framework was utilized on the NASA X-57 DEP aircraft to showcase how different power management strategies can be tested and evaluated on various mission scenarios. This new framework creates the groundwork for exploration and comparison of unconventional architectures under varying power management scenarios at early design stages by enabling analysis-based architecture selections driven by requirements. This capability is particularly useful for the design and performance evaluation of multi-mission UAVs where adaptation of different power management strategies to individual missions can be extremely critical in military applications. The framework is also recommended to be utilized for modular UAVs where the propulsion architecture can be modified based on the mission requirements (e.g. by utilizing swappable battery packs) which would bring new mission capabilities. The modifications in propulsion architecture can be captured through the

Architecture Matrices, and the changing capabilities can be simulated through the Operation Matrices. As future work, the authors will explore the architecture design and operation space of electrified, multi-mission aircraft.

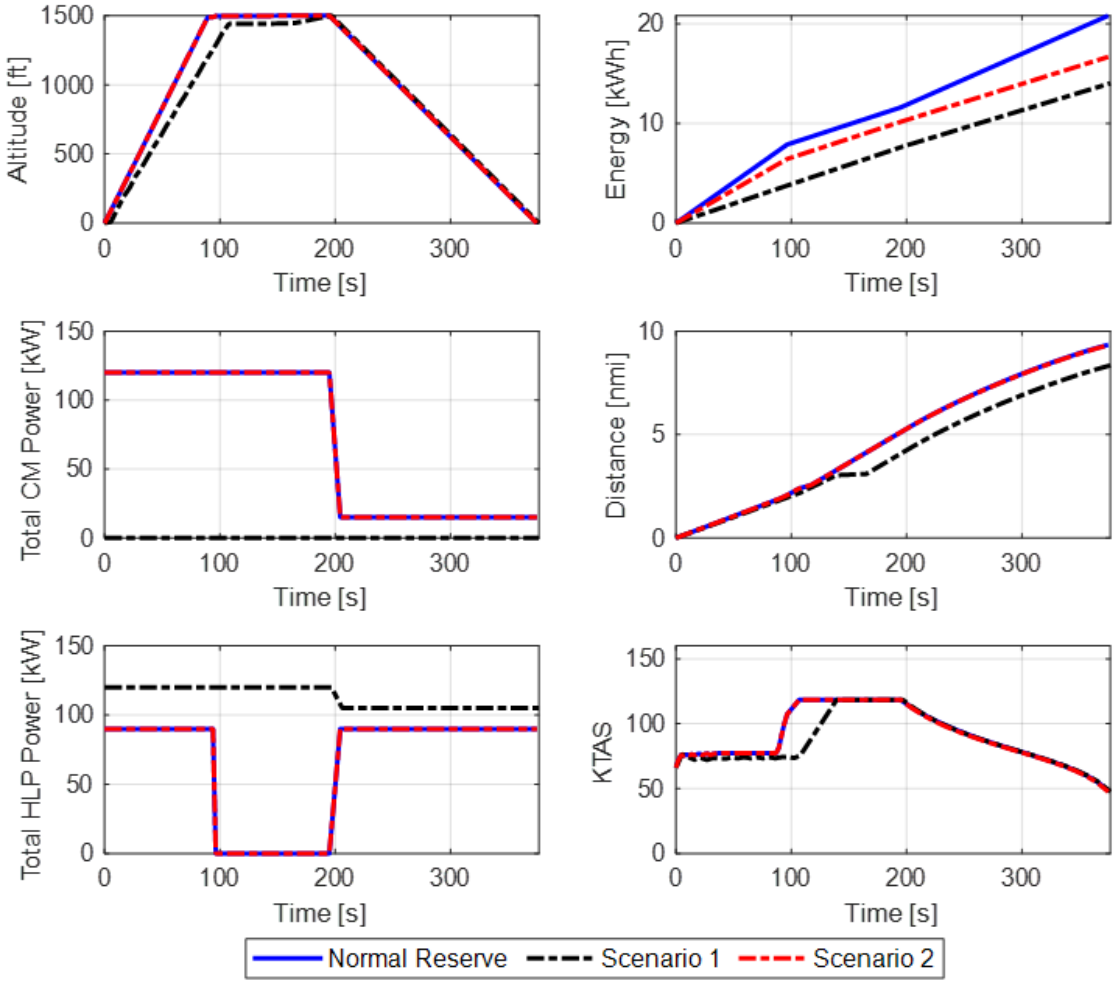

Figure 3-4 Mission performance and power schedule comparisons of normal reserve mission and motor failure scenarios

REFERENCES

Borer, N.K., Nickol, C.L., Jones, F., Yasky, R., Woodham, K., Fell, J., Litherland, B., Loyselle, P., Provenza, A., Kohlman, L. and Samuel, A., 2016. “Overcoming the adoption barrier to electric flight”, In *54th AIAA Aerospace Sciences Meeting* (p. 1022).

Chin, J., Schnulo, S.L. and Smith, A., 2017. Transient Thermal Analyses of Passive Systems on SCEPTOR X-57. In *17th AIAA Aviation Technology, Integration, and Operations Conference* (p. 3784).

Cinar, G., (2018), “A Methodology for dynamic sizing of electric power generation and distribution architectures” (Doctoral dissertation, Georgia Institute of Technology).

Cinar, G., Mavris, D.N., Emeneth, M., Schneegans, A. and Fefermann, Y., (2017), “Development of parametric power generation and distribution subsystem models at the conceptual aircraft design stage”, In *55th AIAA Aerospace Sciences Meeting* (p. 1182).

Clarke, S., Redifer, M., Papathakis, K., Samuel, A. and Foster, T., (2017), June. “X-57 power and command system design”, In *2017 IEEE Transportation Electrification Conference and Expo (ITEC)* (pp. 393-400). IEEE.

Deere, K.A., Viken, J.K., Viken, S., Carter, M.B., Wiese, M. and Farr, N., (2017), “Computational Analysis of a Wing Designed for the X-57 Distributed Electric Propulsion Aircraft”, In *35th AIAA Applied Aerodynamics Conference* (p. 3923).

Gibbs, Y. (2018), "NASA Armstrong Fact Sheet: NASA X-57 Maxwell", available at: https://www.nasa.gov/centers/armstrong/news/FactSheets/FS-109.html (accessed 17 May 2019).

Isikveren, A.T., Seitz, A., Vratny, P.C., Pornet, C., Plötner, K.O. and Hornung, M., (2012), September. “Conceptual studies of universally-electric systems architectures suitable for transport aircraft”, In *Deutscher Luft-und Raumfahrt Kongress*. Berlin: DLRK.

Larminie, J. and Lowry, J., 2012. *Electric vehicle technology explained*. John Wiley & Sons.

Nam, T., Soban, D. and Mavris, D., (2005), “A generalized aircraft sizing method and application to electric aircraft”, In *3rd International Energy Conversion Engineering Conference* (p. 5574).

Schnulo, S.L., Chin, J., Falck, R.D., Gray, J.S., Papathakis, K.V., Clarke, S.C., Reid, N. and Borer, N.K. (2018), “Development of a multi-segment mission planning tool for SCEPTOR X-57”, In *2018 Multidisciplinary Analysis and Optimization Conference* (p. 3738).

Siemens, Airbus and Rolls-Royce (2017), “Airbus, Rolls-Royce, and Siemens team up for electric future”, available at:
https://www.siemens.com/press//pool/de/pressemitteilungen/2017/corporate/PR2017110098COEN.pdf
(accessed 17 May 2019).

Welstead, J. and Felder, J.L., (2016), “Conceptual design of a single-aisle turboelectric commercial transport with fuselage boundary layer ingestion”, In *54th AIAA Aerospace Sciences Meeting* (p. 1027).

APPENDIX

This section shows the Equations (4)-(7) expanded for the series-parallel configuration given in Figure 2.3-1-(c).

$$A_{TS}^{P} = \begin{bmatrix} P_{TS-1,1} \\ \vdots \end{bmatrix}_{nx1} = \begin{bmatrix} TV_{req,,1} \\ \vdots \end{bmatrix}_{nx1} [1]_{nx1}$$

$$A_{PS}^{P^*} = \begin{bmatrix} P_{PS-1,1}^{*} & P_{PS-2,1}^{*} \\ \vdots & \vdots \end{bmatrix}_{nx2} = \begin{bmatrix} P_{TS-1,1} \\ \vdots \end{bmatrix}_{nx1} ([\lambda_{TS-1,PS-1} \quad \lambda_{TS-1,PS-2}]_{1x2} \oslash [\Pi_{TS-1,PS-1} \quad \Pi_{TS-1,PS-2}]_{1x2})$$

$$A_{PS}^{P} = \begin{bmatrix} P_{PS-1,1} & P_{PS-2,1} \\ \vdots & \vdots \end{bmatrix}_{nx2} = \begin{bmatrix} P_{PS-1,1}^{*} & P_{PS-2,1}^{*} \\ \vdots & \vdots \end{bmatrix}_{nx2} \left(\begin{bmatrix} 1 & 0 \\ \lambda_{PS-2,PS-1} & 1 \end{bmatrix}_{1x2} \oslash \begin{bmatrix} 1 & 1 \\ \Pi_{PS-2,PS-1} & 1 \end{bmatrix}_{1x2} \right)$$

$$A_{ES}^{P} = \begin{bmatrix} P_{ES-1,1} & P_{ES-2,1} \\ \vdots & \vdots \end{bmatrix}_{nx2} = \begin{bmatrix} P_{PS-1,1} & P_{PS-2,1} \\ \vdots & \vdots \end{bmatrix}_{nx2} \left(\begin{bmatrix} \lambda_{PS-1,ES-1} & 0 \\ 0 & \lambda_{PS-2,ES-2} \end{bmatrix}_{1x2} \oslash \begin{bmatrix} \Pi_{PS-1,ES-1} & 1 \\ 1 & \Pi_{PS-2,ES-2} \end{bmatrix}_{1x2} \right)$$

Thus:

$$P_{TS-1,1} = TV_{req,1}$$

$$P_{PS-1,1}^{*} = \frac{P_{TS-1,1}\lambda_{TS-1,PS-1}}{\Pi_{TS-1,PS-1}}; \qquad P_{PS-2,1}^{*} = \frac{P_{TS-1,1}\lambda_{TS-1,PS-2}}{\Pi_{TS-1,PS-2}}$$

$$P_{PS-1,1} = P_{PS-1,1}^{*} + \frac{P_{PS-2,1}^{*}\lambda_{PS-2,PS-1}}{\Pi_{PS-2,PS-1}}; \qquad P_{PS-2,1} = P_{PS-2,1}^{*}$$

$$P_{ES-1,1} = \frac{P_{PS-1,1}\lambda_{PS-1,ES-1}}{\Pi_{PS-1,ES-1}}; \qquad P_{ES-2,1} = \frac{P_{PS-2,1}\lambda_{PS-2,ES-2}}{\Pi_{PS-2,ES-2}}$$